

H₂BZmacropa-NCS: A Bifunctional Chelator for Actinium-225 Targeted Alpha Therapy

Karthika J. Kadassery,^{§,†} A. Paden King,^{§,‡} Stanley Fayn,[‡] Kwamena E. Baidoo,[‡] Samantha N. MacMilan,[†] Freddy E. Escoria,^{‡,*} and Justin J. Wilson^{†,**}

[†]Department of Chemistry and Chemical Biology, Cornell University, Ithaca, New York 14853, United States.

[‡]Center for Cancer Research, National Cancer Institute, National Institutes of Health, Bethesda, Maryland 20892, United States.

[§]Denotes Equally Contributing Authors

^{*}Freddy Escoria, 10 Center Drive, Building 10, Room 1B54, Bethesda, Maryland 20892, (240) 858-3062, freddy.escoria@nih.gov

^{**}Justin Wilson, G50A Baker Laboratory, Cornell University, Ithaca, New York 14853, (607) 255-4344, jjw275@cornell.edu

ABSTRACT: Actinium-225 (²²⁵Ac) is one of the most promising radionuclides for targeted alpha therapy (TAT). With a half-life of 9.92 days and a decay chain that emits four high energy α particles, ²²⁵Ac is well-suited for TAT when conjugated to macromolecular targeting vectors that exhibit extended *in vivo* circulation times. The implementation of ²²⁵Ac in these targeted constructs, however, requires a suitable chelator that can bind and retain this radionuclide *in vivo*. Previous work has demonstrated the suitability of a diaza-18-crown-6 macrocyclic chelator H₂macropa for this application. Building upon these prior efforts, in this study, two rigid variants of H₂macropa, which contain either one (H₂BZmacropa) or two (H₂BZ₂macropa) benzene rings within the macrocyclic core, were synthesized and investigated for their potential use for ²²⁵Ac TAT. The coordination chemistry of these ligands with La³⁺, used as a non-radioactive model for Ac³⁺, was carried out. Both NMR spectroscopic and X-ray crystallographic studies of the La³⁺ complexes of these ligands revealed similar structural features as those found for the related complex of H₂macropa. Thermodynamic stability constants of the La³⁺ complexes, however, were found to be one and two orders of magnitude lower than those of H₂macropa for H₂BZmacropa and H₂BZ₂macropa, respectively. The decrease in thermodynamic stability was rationalized via the use of density functional theory calculations. ²²⁵Ac radiolabeling and serum stability studies with H₂BZmacropa showed that this chelator compares favorably with H₂macropa. Based on these promising results, a bifunctional version of this chelator, H₂BZmacropa-NCS, was synthesized and conjugated to the antibody codrituzumab (GC33), which targets the liver cancer biomarker glypican-3 (GPC3). The resulting GC33-BZmacropa conjugate and an analogous GC33-macropa were evaluated for their ²²⁵Ac radiolabeling efficiencies, antigen-binding affinity, and *in vivo* biodistribution in HepG2 liver cancer tumor-bearing mice. Although both conjugates were comparably effective in their radiolabeling efficiencies, [²²⁵Ac]Ac-GC33-BZmacropa showed slightly poorer serum stability and biodistribution than [²²⁵Ac]Ac-GC33-macropa. Together, these results establish H₂BZmacropa-NCS as a new bifunctional chelator for the preparation of ²²⁵Ac radiopharmaceuticals.

INTRODUCTION

The 2013 FDA approval of ²²³RaCl₂ (Xofigo®) for the management of bone metastases in castration-resistant prostate cancer (mCRPC) patients has heralded a renaissance in targeted alpha therapy (TAT), a treatment

modality that uses the high linear energy transfer of alpha (α) particles to annihilate cancer cells.¹ Despite the success of this drug, the development of new radiopharmaceutical agents employing ²²³Ra has been hindered by the difficult chelation chemistry of this ion.² Fortunately, a number of other α -emitting radionuclides, such as ²²⁷Th, ²²⁵Ac, ²¹³Bi, ²¹²Bi, ²¹²Pb, and ²¹¹At, have suitable properties for use in TAT.³ Among these radionuclides, ²²⁵Ac has demonstrated particular promise due to advances in its large-scale production, its ideal 9.92-day physical half-life for conjugation to long-lived biomolecules, and high cytotoxic potency, which arises from the four α particles emitted through its decay chain.^{4,5} Clinical trials of ²²⁵Ac small-molecule^{6,7} and antibody⁸ conjugates are underway, and early results have been promising.

A significant limitation in the development of new ²²⁵Ac-based TAT radiopharmaceutical agents has arisen from the difficulty in identifying suitable chelating agents for the large Ac³⁺ ion.⁵ Although acyclic chelators such as ethylenediamine tetraacetic acid (H₄EDTA) and diethylenetriamine pentaacetic acid (H₅DTPA) have been

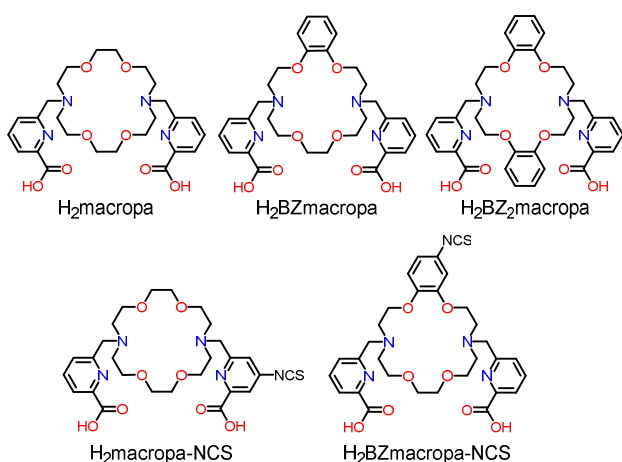


Chart 1. Chelators Discussed in this Work.

Table 1. Protonation Constants of Various Chelators and the Thermodynamic Stability Constants of Corresponding La^{3+} Complexes Determined by pH Potentiometry (25 °C and $I = 0.1 \text{ M KCl}$).

	H₂macropa	H₂BZmacropa	H₂BZ₂macropa	H₄DOTA	H₅DTPA	H₄EDTA
$\log K_1$	7.41(1) ^c	7.06(2)	6.89(7)	11.14 ^d	10.45 ^e	10.17 ^e
$\log K_2$	6.85(1) ^c	6.41(1)	6.11(3)	9.69 ^d	8.53 ^e	6.11 ^e
$\log K_3$	3.32(1) ^c	3.35(2)	3.36(3)	4.84 ^d	4.28 ^e	2.68 ^e
$\log K_4$	2.36(1) ^c	2.41(9)	2.26(9)	3.95 ^d	2.65 ^e	2.00 ^e
$\log K_5$	1.69(1) ^c		-		1.82 ^e	1.5 ^e
$\log K_{\text{LaL}}$	14.99(2)^c	13.99(5)	12.04(6)	21.7(1)^d	19.48^e	15.46^e
$\log K_{\text{LaHL}}$	2.28(3)^c	-	-	2.5(2)^d	-	2.24^e
$\log K'_{\text{La}}^{\text{a}}$	14.63	13.81	11.92	15.67	15.27	12.67
$p\text{La}^{\text{b}}$	15.58	14.77	12.87	16.62	16.22	13.62

^aConditional stability constants ($\log K'_{\text{M}}$) at pH 7.4, 25 °C, and $I = 0.1 \text{ M KCl}$

^bpM values calculated from $-\log [\text{M}]_{\text{free}}$ ($[\text{M}]_{\text{total}} = 10^{-6} \text{ M}$, $[\text{L}]_{\text{total}} = 10^{-5} \text{ M}$, pH 7.4, 25 °C, and $I = 0.1 \text{ M KCl}$)

^c0.1 M KCl, ref²¹. ^d0.1 M KCl, ref²². ^e0.1 M, ref²³.

shown to possess high affinity for the $^{225}\text{Ac}^{3+}$ ion, the resulting complexes are labile, leading to release of the free metal ion in biological systems.⁹ By contrast, many Ac^{3+} complexes of macrocyclic chelators are substantially more inert. For example, the macrocyclic chelator tetraazacyclododecane-1,4,7,10-tetraacetic acid (H₄DOTA) has been used successfully for both small molecule and antibody ^{225}Ac -radioconjugates, albeit with some significant challenges. For example, radiolabeling of H₄DOTA with ^{225}Ac either requires high temperature, which are incompatible with macromolecular biomolecules like antibodies, or long incubation times, which yields constructs with relatively low-specific-activities.^{10–14} Furthermore, serum stability studies have shown that the [^{225}Ac]Ac-DOTA complex dissociates over time,¹⁵ a property that is corroborated by animal studies that show deposition of ^{225}Ac in the liver and femur after the administration of DOTA-based conjugates.¹⁶ These drawbacks have sparked efforts to develop superior bifunctional chelators for ^{225}Ac .

To accommodate the large ionic radius of Ac^{3+} , researchers have targeted alternative ligands that contain greater than 8 donor atoms to saturate its coordination sphere. For instance, the macrocycles bispa,¹⁷ crown,¹⁸ macrodipa, and py-macrodipa¹⁹ as well as the acyclic chelators octapa,¹⁵ py4pa²⁰ and phospha¹⁵ have all successfully radiolabeled $^{225}\text{Ac}^{3+}$ at room temperature in < 60 min. However, not all these chelators form sufficiently stable complexes with ^{225}Ac for biological use.

Among the potential alternative to H₄DOTA, the diaza-18-crown-6 macrocyclic chelator H₂macropa (Chart 1) has shown significant promise for ^{225}Ac chelation in TAT applications.^{24,25} This compound is unique by virtue of its high selectivity for large over small lanthanide ions,²¹ a property that makes it favorable for use with the large Ac^{3+} ion. In contrast to H₄DOTA, this chelator can quantitatively radiolabel ^{225}Ac at room temperature in 5 mins and form complexes that are sufficiently stable for long-term biological applications. The success of this chelator for use with ^{225}Ac has been demonstrated by several

studies that have used it in conjunction with small-molecule and antibody-based targeting vectors.^{26–29}

The efficacy of H₂macropa suggests that this structural archetype is valuable for Ac^{3+} chelation. Building upon this scaffold, two new analogues of H₂macropa were investigated. These compounds are rigidified versions of the parent chelator, containing either one (H₂BZmacropa) or two (H₂BZ₂macropa) benzene rings within the 18-membered macrocycle (Chart 1). We hypothesized that the decreased conformational flexibility of these new analogues would preorganize them for more effective and stable chelation of the Ac^{3+} ion.^{30–35} This study presents a comprehensive comparative investigation of these new chelators with respect to their La^{3+} and Ac^{3+} -complexing properties. Furthermore, a bifunctional chelator, H₂BZmacropa-NCS, and its conjugate to the glyican-3 (GPC3)-targeting antibody codrituzumab³⁶ (GC33) were prepared. The resulting ^{225}Ac -labeled GC33-BZmacropa conjugate was then assessed in an in vivo mouse model of liver cancer. Collectively, the results from this study highlight the importance of ligand design principles in developing effective chelating agents for TAT applications.

RESULTS AND DISCUSSION

Chelate Syntheses. The previously reported ligands, H₂macropa²¹ and H₂BZmacropa,³⁷ and the novel ligand H₂BZ₂macropa were synthesized via adaptations of procedures that have been used to access related macrocyclic chelators.³⁸ Briefly, the ligands were synthesized by the alkylation of the corresponding diaza-18-crown-6 macrocycle at the secondary amine nitrogen with 6-(bromomethyl)pyridine-2-carboxylic acid methyl ester followed by acid hydrolysis of the ester functional groups (Scheme S1–S2). The ligands were fully characterized by NMR spectroscopy, mass spectrometry, elemental analysis, and analytical HPLC (Figures S1–S29).

Coordination Chemistry with La^{3+} . Because no stable isotopes of Ac^{3+} exist, the coordination chemistries

of $\text{H}_2\text{BZmacropa}$ and $\text{H}_2\text{BZ}_2\text{macropa}$ were investigated using La^{3+} . As the largest lanthanide, this ion has a similar ionic radius, hydrolysis constant, and hard-soft acid-base properties to Ac^{3+} , thus rendering it a suitable model.^{5,39} Treatment of equimolar ratios of LaCl_3 with each compound in water at neutral pH followed by salt metathesis with KPF_6 led to the precipitation of the $[\text{LaL}(\text{H}_2\text{O})]\text{PF}_6$ complexes, which were crystallized via the slow evaporation of concentrated aqueous solutions at room temperature. The structures of these complexes (Figure 1), as determined by X-ray crystallography, are comparable to that of $[\text{La}(\text{macropa})(\text{H}_2\text{O})]^+$.²⁴ In all three complexes, the La^{3+} center attains an 11-coordinate geometry with 10 donors provided by the macrocyclic ligands and the 11th arising from an inner-sphere water molecule that interpenetrates the macrocyclic core.

Within the macropa^{2-} and BZmacropa^{2-} structures, the metal ion sits above the mean plane of the O-atoms in the macrocycle (O1–O4), resulting in near linear N1–La–N2 angles of 178.04° and 172.41° , respectively. By contrast, the structure of $[\text{La}(\text{BZ}_2\text{macropa})(\text{H}_2\text{O})]^+$ shows that all the donor atoms of the macrocyclic base reside in a plane below the La^{3+} center, rendering the N1–La–N2 angle to be much more acute (148.77°). This distortion is most likely a consequence of the presence of the two rigid benzene groups, which lead to additional strain in the macrocycle of $\text{BZ}_2\text{macropa}^{2-}$ upon coordination to the La^{3+} backbone.

In addition to this distortion, there are also significant differences with respect to the interatomic distances between the donor atoms and the La^{3+} center within these structures. For example, the inner coordination sphere of

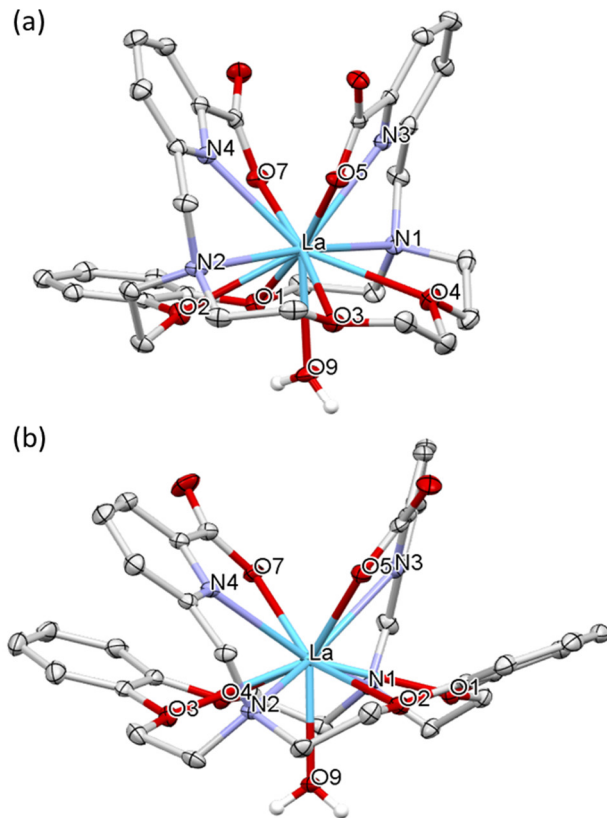


Figure 1. Crystal structures of (a) $[\text{La}(\text{BZmacropa})(\text{H}_2\text{O})]\text{PF}_6$ and (b) $[\text{La}(\text{BZ}_2\text{macropa})(\text{H}_2\text{O})]\text{PF}_6$. Thermal ellipsoids are drawn at the 50% probability level. Outer-sphere solvents, counter-anions, and hydrogen atoms attached to carbon centers are omitted for clarity. Color scheme: La = blue; O = red; N = violet; C = grey.

the La^{3+} ion in the BZmacropa complex is relatively asymmetric; the La–N distances on the macrocycle are 2.857 and 2.957 Å, representing a significant difference of 0.1 Å. Furthermore, the La–O distances from the aryl ether oxygens of the macrocycle are significantly disparate at 2.772 and 3.058 Å. By contrast, the crystal structure of $[\text{La}(\text{BZ}_2\text{macropa})(\text{H}_2\text{O})]^+$ is relatively symmetric with chemically equivalent donor atoms interacting with the La^{3+} center at similar distances. However, the La–O distances within the macrocycle fall between 2.83 and 2.96 Å. By contrast, the crystal structure of $[\text{La}(\text{macropa})]^+$ has La–O distances that are much shorter (between 2.70 and 2.79 Å). Thus, the aryl ethers donors conferred by the benzene ring appear to interact more weakly than the aliphatic etheral donors, as evidenced by the longer interatomic distances in the former.

Solution Thermodynamics with La^{3+} . To assess the effects of the presence of the rigid benzene groups on the metal-binding properties of $\text{H}_2\text{BZmacropa}$ and

$\text{H}_2\text{BZ}_2\text{macropa}$, the thermodynamic stabilities of their La^{3+} complexes were measured via pH potentiometric titrations. The protonation constants of $\text{H}_2\text{BZmacropa}$ and $\text{H}_2\text{BZ}_2\text{macropa}$ and the stability constants of their La^{3+} complexes are collected in Table 1. For both the chelators, a total of four protonation constants were observed over a pH range of 2.5–11.3. The first and the second protonation constants most likely correspond to the sequential protonation of the macrocyclic amine nitrogen atoms, whereas the third and the fourth protonation constants are assigned to the protonation at the picolinate pendent arms. Although there are six basic sites on the chelators, the fifth and sixth protonation constants could not be determined using the pH ranges employed in these titrations. The sum of the first and second protonation constants of the rigid compounds are 0.8 and 1.3 log units, respectively, lower than that of macropa, indicating that the addition of phenyl groups increases the acidity of the macrocycles. This result is an expected consequence of the electron-withdrawing nature of the phenyl groups and is consistent with previously reported data on similar macrocyclic chelators.^{40–42} It should be noted that the protonation constants for $\text{H}_2\text{BZmacropa}$ have been previously reported,³⁷ and these values—in particular the most basic protonation constant—differ somewhat from those measured in this study. The use of different media for ionic strength (0.1 M KCl vs 0.1 M KNO_3) could partly explain these discrepancies. In any case, the pH potentiometric titrations in the present study were carried out in triplicate and are reported with a high degree of confidence.

After obtaining the protonation constants, the La^{3+} stability constants ($\log K_{\text{LaL}}$) of the $\text{H}_2\text{BZmacropa}$ and $\text{H}_2\text{BZ}_2\text{macropa}$ complexes were determined by pH potentiometric titrations (Table 1). The $\log K_{\text{LaL}}$ values decrease upon the addition of phenyl groups to the macrocyclic backbone, following the sequence $\log K_{\text{Lamacropa}} > \log K_{\text{LaBZmacropa}} > \log K_{\text{LaBZ}_2\text{macropa}}$. The stability constant for the La^{3+} complex of $\text{H}_2\text{BZmacropa}$ ($\log K_{\text{LaL}} = 13.99$) is approximately 1 log unit lower than that of $\text{H}_2\text{macropa}$ ($\log K_{\text{LaL}} = 14.99$). The introduction of a second phenyl group in $\text{H}_2\text{BZ}_2\text{macropa}$ leads to an even greater destabilization of the complexes, as reflected by $\log K_{\text{LaL}}$ ($\log K_{\text{LaL}} = 12.04$) that is almost 2 log units lower than that of $\text{H}_2\text{BZmacropa}$. In order to account for the effect of protonation equilibria of the ligands on complex stability, the conditional stability constants ($\log K'_{\text{LaL}}$) and pLa (the negative log of the free metal concentration in a solution containing 10^{-6} M metal ion and 10^{-5} M chelator) at biologically relevant $\text{pH} = 7.4$ were calculated (Table 1). The trends in these conditional stability constants follow those of the absolute values with $\log K'_{\text{Lamacropa}} = 14.63$, $\log K'_{\text{LaBZmacropa}} = 13.81$, and $\log K'_{\text{LaBZ}_2\text{macropa}} = 11.92$. Although ligand rigidification should in principle lead to enhanced metal complex stability, this effect may depend on several factors including the type of metal employed. For example, a previous study of ethylene glycol-bis(β -aminoethyl

ether)-N,N,N',N'-tetraacetic acid (H_4EGTA) and an analogue of H_4EGTA with a phenyl backbone showed that enhanced stability was exhibited for the Ca^{2+} complex, but stability decreased for the La^{3+} complex.⁴² The reduced stability observed in the cases of $\text{H}_2\text{BZmacropa}$ and $\text{H}_2\text{BZ}_2\text{macropa}$ may thus be a consequence of several different factors.

Although the overall LaL stability constants for the rigid ligands are lower than that of $\text{H}_2\text{macropa}$, the absolute values exceed 10, suggesting that they form sufficiently strong complexes for use in ^{225}Ac TAT.

DFT Calculations. In order to better understand the La^{3+} stability constant trends, density functional theory (DFT) was employed. The geometries of $[\text{La}(\text{macropa})(\text{OH}_2)]^+$, $[\text{La}(\text{BZmacropa})(\text{OH}_2)]^+$, and $[\text{La}(\text{BZ}_2\text{macropa})(\text{OH}_2)]^+$ were first optimized. The resulting structures are qualitatively similar to the experimentally determined X-ray crystal structures, but exhibit a systematic elongation of the La donor atom distances within the macrocycles of approximately 0.05–0.10 Å. More importantly, however, the relatively asymmetry of $[\text{La}(\text{BZmacropa})(\text{OH}_2)]^+$ is captured by the DFT optimization, thus validating this level of theory. With suitably optimized structures, the ΔG° values for the transchelation reaction between $[\text{La}(\text{macropa})(\text{H}_2\text{O})]^+$ and either BZmacropa^{2-} or $\text{BZ}_2\text{macropa}^{2-}$ were calculated.

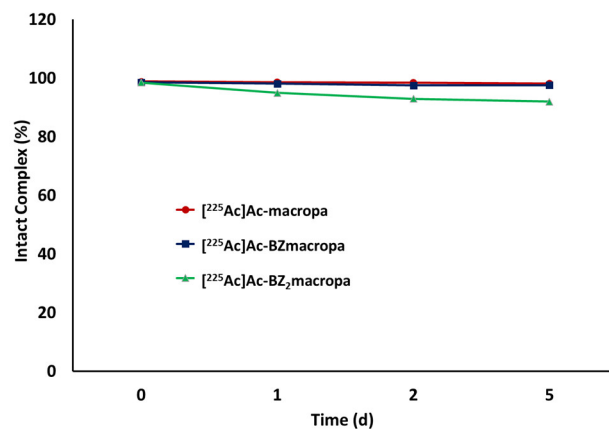
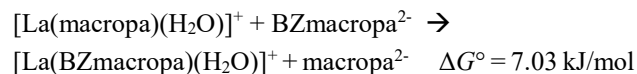
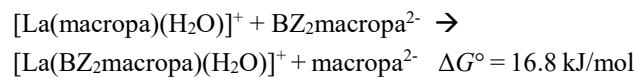


Figure 2. Stability of ^{225}Ac complexes in human serum over time. Stability was measured using ITLC condition 1 as detailed in the Supporting Information.



For both of these reactions, the ΔG° was found to be > 0 , indicating that both BZmacropa^{2-} and $\text{BZ}_2\text{macropa}^{2-}$ form less thermodynamically stable complexes with La^{3+} than

macropa²⁻. Furthermore, ΔG° for the transchelation with BZ₂macropa²⁻ was approximately 10 kJ/mol greater than that for BZmacropa²⁻. Collectively, these computational results are consistent with our experimental data that show BZ₂macropa²⁻ forms the least stable La³⁺ complex of these three ligands.

Having validated our computational method against the experimental results, we analyzed the different factors that contribute to ΔG° for these reactions. As described in the Supporting Information (Section S1.6), ΔG° can be expressed as the sum $\Delta\Delta G_S^\circ + \Delta\Delta G_B^\circ$, where $\Delta\Delta G_S^\circ$ is the relative ligand strain energy and $\Delta\Delta G_B^\circ$ is the relative metal ion-binding energy (see SI section S1.6 for more details).^{35,38,43,44} The strain energy (ΔG_S°) is defined as the free energy change required to distort the geometrically relaxed free ligand (L) to a conformation that is suitable for metal ion-binding (L_{strain} , eq. S1), and the binding energy (ΔG_B°) is defined as the free energy change associated with the incorporation of the La³⁺ ion into the ligand in its preorganized metal-binding conformation (eq. S2). The relative ($\Delta\Delta G$) values, compared to macropa²⁻, are given below.

$$\Delta\Delta G_S^\circ (\text{BZmacropa}^{2-}) = -13.95 \text{ kJ/mol}$$

$$\Delta\Delta G_B^\circ (\text{BZmacropa}^{2-}) = 20.98 \text{ kJ/mol}$$

$$\Delta\Delta G_S^\circ (\text{BZ}_2\text{macropa}^{2-}) = -14.41 \text{ kJ/mol}$$

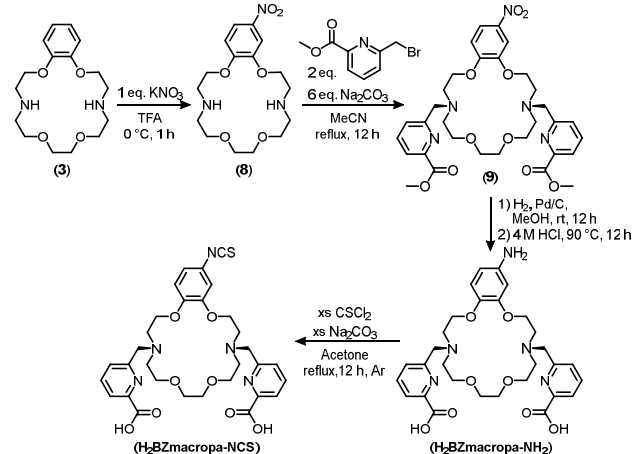
$$\Delta\Delta G_B^\circ (\text{BZ}_2\text{macropa}^{2-}) = 31.17 \text{ kJ/mol}$$

For both BZmacropa²⁻ and BZ₂macropa²⁻ $\Delta\Delta G_S^\circ$ are negative, indicating that these compounds undergo a significantly smaller free energy penalty for attaining an appropriate metal-binding conformation than macropa²⁻. This result is consistent with role of the rigid benzene groups in enhancing the metal-binding preorganization of these ligands. By contrast, the $\Delta\Delta G_B^\circ$ values for both rigid chelators are positive, a result that suggests that macropa forms stronger binding interactions with the La³⁺ ion. The weaker binding energies of H₂BZmacropa and H₂BZ₂macropa, compared to H₂macropa, is most likely a consequence of their decreased basicity and donor strength. As noted above, the electron-withdrawing phenyl groups embedded in the macrocycle decreases their basicity, as determined experimentally via protonation constant measurements. This decreased basicity also renders them less effective Lewis bases for binding with La³⁺. To further verify this conclusion computationally, the ΔG° for a simple model ligand substitution reaction on La³⁺ was calculated. In this substitution reaction, the ΔG° values required to displace dimethyl ether, a model for the aliphatic ether donors in H₂macropa, with anisole, an aromatic ether that models the donors on H₂BZmacropa and H₂BZ₂macropa. These calculations revealed that displacement of dimethyl ether by anisole is thermodynamically uphill ($\Delta G^\circ = 17.22 \text{ kJ/mol}$). Thus, the weaker donor strengths of the aromatic ethers is

a plausible explanation for the positive $\Delta\Delta G_B^\circ$ determined for H₂BZmacropa and H₂BZ₂macropa. Together, these results reveal a counterbalancing effect of the introduction of the rigid phenyl groups. Although these rigid phenyl groups provide a favorable entropic contribution by preorganizing the ligands for metal binding, their weaker donor strengths provide a poorer enthalpic contribution to La³⁺ binding. For BZmacropa²⁻ and BZ₂macropa²⁻, the weaker binding strength outweighs the benefits obtained in ligand preorganization.

Radiolabeling and Stability Studies. With the comprehensive characterization of the La³⁺ complexes of BZmacropa²⁻ and BZ₂macropa²⁻, which revealed them to be effective ligands for this ion, their ability to chelate Ac³⁺ was investigated. The chelators (~300 μM) were incubated at room temperature with 70 μCi (2.6 Mbq) [²²⁵Ac]Ac(NO₃)₃ in water containing NH₄OAc (0.1 M) at pH 5.5. Under these conditions, both ligands, as well as macropa, quantitatively radiolabeled ²²⁵Ac³⁺ in only 30 min, resulting in high specific activities of approximately 7.5 Ci/g (260 TBq/g). Instant thin-layer chromatography (ITLC) chromatograms, showing the complex formation for these ligands and macropa, are in the Supporting Information, Figures S63–S66. These results, particularly the room temperature radiolabeling, confirm the high efficacy of expanded macrocyclic ligands like macropa²⁻ for chelation of the large Ac³⁺ ion.

Having demonstrated the rapid and high specific activity radiolabeling with H₂BZmacropa and H₂BZ₂macropa, the stabilities of the resulting Ac³⁺ complexes in whole human serum at 37°C were evaluated (Fig-



Scheme 1. Synthetic scheme for H₂BZmacrop-NCS.

ure 2, S70–S72). Under these conditions, all complexes were >90% intact after 5 days. Even with this high uniform stability among the complexes several trends could be discerned. Specifically, increasing stability of the complexes followed the order BZ₂macropa²⁻ < BZmacropa²⁻ < macropa²⁻. This trend matches that observed with the thermodynamic stability constant data of the La³⁺ complexes that was rationalized with DFT calculations, described above.

Bifunctional Chelator, H₂BZmacropa-NCS.

The high stability of the ²²⁵Ac complex of BZmacropa prompted us to prepare a bifunctional version of this chelator. For this purpose, we targeted the chelator H₂BZmacropa-NCS (**Chart 1**), which contains an amine-reactive isothiocyanate group appended to the phenyl ring of the macrocyclic backbone. The synthesis of this compound (Scheme 1) commenced from the macrocycle **3** which upon treatment with 1 equiv. of KNO₃ in trifluoroacetic acid afforded the monosubstituted nitro-product **8** in near quantitative yield. The addition of the pendent arms to the nitrated macrocycle was accomplished by alkylation of **8** at the secondary amine nitrogen with 6-(bromomethyl)pyridine-2-carboxylic acid methyl ester. Reduction of the nitrated compound **9** using H₂ over Pd/C followed by acid hydrolysis of the ester functional groups yielded H₂BZmacropa-NH₂. Finally, the isothiocyanate functional group was installed onto the macrocycle via the treatment of H₂BZmacropa-NH₂ with excess thiophosgene. The compound H₂BZmacropa-NCS was fully characterized by NMR spectroscopy, mass spectrometry, and analytical HPLC (Figures S30-S40).

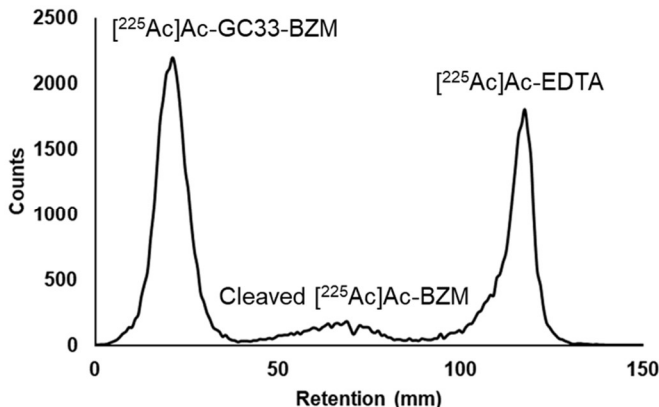
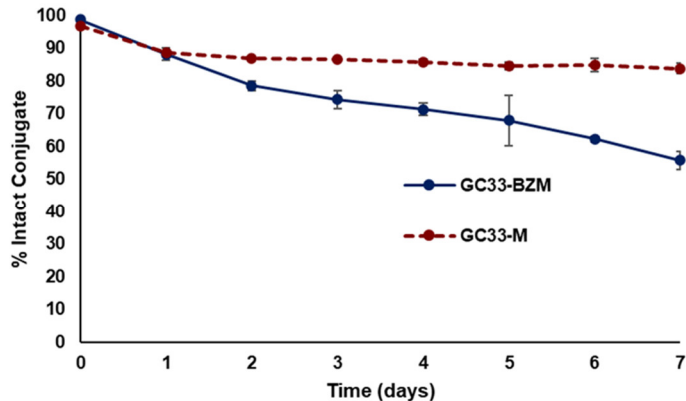


Figure 3. (Left) ITLC chromatogram of ²²⁵Ac]Ac-GC33-BZM after 7 day incubation in human serum at 37°C. (Right) Stability over time of ²²⁵Ac]Ac-GC33-BZM and ²²⁵Ac]Ac-GC33-M in human serum. Data points are the average of 3 independent samples and error bars represent the standard deviation.

A key difference between the first-generation bifunctional chelator H₂macropa-NCS (**Chart 1**) and H₂BZmacropa-NCS is the location of the amine-reactive –NCS group. On H₂BZmacropa-NCS, this functional group is attached to the macrocycle backbone, whereas for H₂macropa-NCS it is on one of the picolinate pendent arms. Consequently, the synthesis of the H₂BZmacropa-NCS is more modular in that it proceeds through intermediate **8**, which can potentially be functionalized with a diverse range of different pendent donor arms to access a library of different bifunctional chelators. Furthermore, the H₂BZmacropa-NCS is relatively easier to synthesize as compared to H₂macropa-NCS. For instance, the synthesis of H₂macropa-NCS involves a 9-step pathway starting from the macrocycle, while the synthesis of H₂BZmacropa-NCS is carried out in 4–5 steps. The location of the –

NCS functional group also has important effects on its hydrolytic stability. For instance, a solution of H₂macropa-NCS in pH 9.1 NaHCO₃ buffer at room temperature completely hydrolyzes to the amine H₂macropa-NH₂ in approximately 5 h (*t*_{1/2} = 1.25 h). Under the same conditions, the hydrolysis of H₂BZmacropa is significantly slower (*t*_{1/2} = 56 h), requiring over a week for near complete formation of the amine. The location of the –NCS group of H₂macropa-NCS directly on the electron-deficient picolinate group increases its electrophilicity, rendering it more reactive and less stable than the –NCS group of H₂BZmacropa-NCS that is linked to a more electron-rich phenyl group. The increased stability of H₂BZmacropa-NCS marks a potential advantage over H₂macropa-NCS, for H₂BZmacropa-NCS may be shipped at room temperature and stored for extended periods of time, rendering it more broadly accessible to researchers across the globe.

Antibody Conjugation. To further evaluate the suitability of H₂BZmacropa-NCS as a bifunctional chelator, this compound was conjugated to the antibody GC33, which targets the GPC3 receptor overexpressed in many liver cancers. The H₂BZmacropa-NCS conjugate of GC33



(GC33-BZM) was prepared using standard antibody-isothiocyanate coupling conditions, which use a slight molar excess (2.5–3 equiv.) of chelator exposed to the antibody in bicarbonate buffer at 37 °C. These conditions were also applied to prepare the macropa conjugate of GC33 (GC33-M) and the H₂BZmacropa-NCS conjugate of Obinutuzumab (OBI-BZM), an antibody that does not bind GPC3. The conjugates were subjected to gel-permeation chromatography to remove any unconjugated bifunctional chelator, and their purities were verified by size-exclusion HPLC (Figures S52–S54).

After purification, the average chelator:antibody ratios were determined. Previous studies have shown that presence of too many covalently attached chelators on antibodies can have negative consequences on their immuno-reactivity and pharmacokinetic properties. As such, a che-

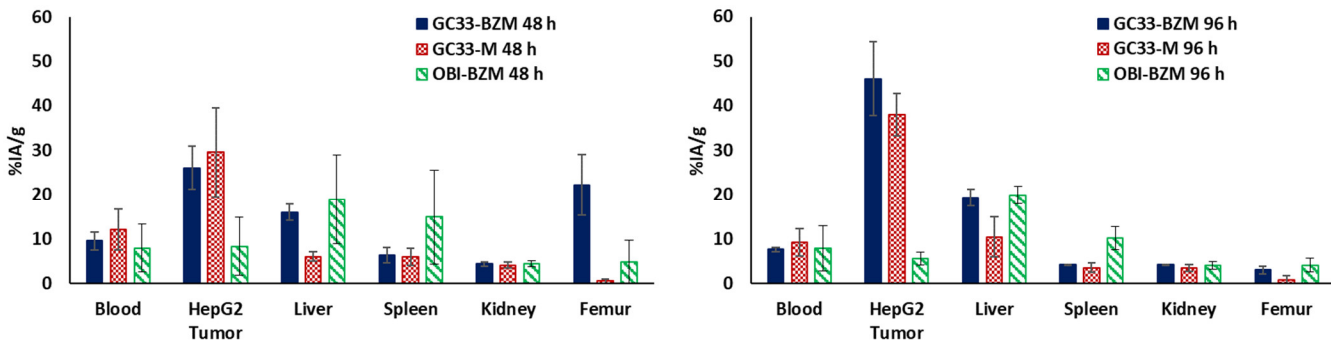


Figure 4. Selected organ biodistribution of ^{225}Ac -labeled GC33-BZM (solid, blue bar), ^{225}Ac -labeled GC33-M (checkered, red bar), and ^{225}Ac -labeled OBI-BZM (striped, green bar) at 48 h (left panel) and 96 h (right panel) after administration ($n = 3\text{--}4$). Full biodistribution data can be found in the SI, Figures S58–S60.

lator:antibody ratio of <5 is generally desirable for radioconjugates.^{45–47} The chelator:antibody ratios were assessed using a modification of the previously reported colorimetric arsenazo assay (Figures S58–S59).⁴⁸ All conjugates were found to have chelator:antibody ratios of approximately 1:1 using this method, indicating that minimal alteration of the antibody was achieved. To provide further verification of these results, the chelator:antibody ratios of GC33-M and GC33-BZM were also determined using UPLC-HRMS. The resulting mass spectra, shown in Figures S55–S57, correspond well with the chelate:antibody ratios determined using the arsenazo method.

Having established the degree of functionalization of these conjugates, we next investigated the impact of this modification on the immunoreactivity of GC33 using bio-layer interferometry (BLI). The exposure of various concentrations of antibody-chelator conjugates to immobilized GPC3 antigen revealed concentration-dependent binding of the antibody to the surface and subsequent dissociation. The combined association and dissociation kinetic data across all concentrations were fit using the global fitting model in the Octet Analysis Studio software (Figures S60–S62). These data revealed K_d values of 0.19, 0.14, and 0.042 nM for GC33-BZM, GC33-M, and GC33 respectively. Taken together, the results show that both GC33-BZM and GC33-M retained comparably high binding affinity for GPC3 that was slightly diminished relative to the free GC33 antibody.

Radiolabeling and Stability Studies with Chelator-Antibody Conjugates. After confirming the identity, purity, and antigen-binding affinity of the antibody conjugates, they were radiolabeled with ^{225}Ac following a previously reported procedure that was used for GC33-M.²⁹ Under these conditions, a solution of antibody conjugates (450 μg) was added to a solution of ^{225}Ac (150 μCi , 5.55 MBq) in aqueous 0.1 M NH_4OAc (pH 5.5). The mixtures were incubated at room temperature for 30 min, after which the completion of the radiolabeling was checked with ITLC (Condition 2). Purification of the radioconjugates by gel permeation chromatography afforded them in $>95\%$ purity, as verified by ITLC (Condition 2) (Figures

S67–S69). The mild conditions and rapid reaction time required for these radiolabelings highlight the suitability of these chelators for antibody radioconjugates of ^{225}Ac . Importantly, the rapid room temperature radiolabeling afforded by these conjugates is critical for minimizing radiolytic damage and thermal aggregation or denaturation of the antibody.

The stabilities of $[^{225}\text{Ac}]\text{Ac-GC33-BZM}$ and $[^{225}\text{Ac}]\text{Ac-GC33-M}$ were evaluated in whole human serum at 37°C over several days (Figure 3, S73–S74). Radio-ITLC analysis (Condition 2) revealed that $[^{225}\text{Ac}]\text{Ac-GC33-M}$ remained $> 90\%$ intact over 7 days, highlighting the excellent stability of the ^{225}Ac complex of the bifunctional macropa-NCS²⁻ chelator. By contrast, the radioconjugate $[^{225}\text{Ac}]\text{Ac-GC33-BZM}$ exhibited marked degradation over the course of the experiment, with approximately 55% intact complex remaining after 7 days. The reduced stability of the $[^{225}\text{Ac}]\text{Ac-GC33-BZM}$ conjugate relative to the unconjugated ligand- ^{225}Ac complex, which showed good stability in human serum, may arise from the electron-withdrawing effect of the thiourea moiety on the ligand backbone, which decreases the donating capacity of the ligand. Notably, for both GC33-M and GC33-BZM radioconjugates, ITLC traces revealed the presence of 3 distinct species in solution: intact conjugate, “free” ^{225}Ac chelated by the mobile phase EDTA, and a third unknown species. This third species reached approximately 10% of the total activity over the course of 1 day, then remained constant throughout the experiment. We hypothesize that this unknown product may be $[^{225}\text{Ac}]\text{Ac-macropa}$ or $[^{225}\text{Ac}]\text{Ac-BZmacropa}$ that has been cleaved from the antibody by radiolysis of the thiourea linker, for extensive radiolysis is often observed in solutions containing ^{225}Ac .^{18,49}

Biodistribution Studies. Despite the lower stability of the $[^{225}\text{Ac}]\text{Ac-GC33-BZM}$ conjugate relative to $[^{225}\text{Ac}]\text{Ac-GC33-M}$, we hypothesized that the former may still have sufficient stability for tumor targeting *in vivo*. To test whether $[^{225}\text{Ac}]\text{Ac-GC33-BZM}$ could successfully target GPC3⁺ tumors *in vivo*, we treated athymic nude mice bearing HepG2 (GPC3⁺) xenografts with 100 nCi (3.7

kBq) of [²²⁵Ac]Ac-GC33-BZM, ²²⁵Ac[Ac]-GC33-M (positive control), and [²²⁵Ac]Ac-OBI-BZM (isotype control). After 48 and 96 h, mice (n = 3–4) were euthanized, and their organs were weighed and counted using a gamma counter after allowing 24 h for daughter isotope equilibration. The % injected-activity per gram (IA/g) in each organ was then calculated (Figure 4, S75–S77). As expected, the isotype control [²²⁵Ac]Ac-OBI-BZM, which does not target the GPC3+ liver cancer xenografts, showed no appreciable tumor uptake at any time point. By contrast, [²²⁵Ac]Ac-GC33-BZM demonstrated clear, specific tumor uptake at both 48 and 96 h post-injection, with tumor signal greater than that of all organs at both time points. Importantly, the tumor uptake of [²²⁵Ac]Ac-GC33-BZM was effectively indistinguishable from that of ²²⁵Ac[Ac]-GC33-M, indicating that these conjugates have comparable targeting capability. “However, the off-target accumulation of ²²⁵Ac in both the liver and femur was higher after administration of [²²⁵Ac]Ac-GC33-BZM than for ²²⁵Ac[Ac]-GC33-M.” A similar degree of liver uptake was also observed in the non-targeted isotype control conjugate [²²⁵Ac]Ac-GC33-BZM. Unchelated ²²⁵Ac has previously been shown to localize to the liver almost exclusively. Therefore, the higher liver uptake measured for both [²²⁵Ac]Ac-GC33-BZM and [²²⁵Ac]Ac-OBI-BZM may be a consequence of partial instability of [²²⁵Ac]Ac-BZmacropa complex under these conditions.⁹ Despite these drawbacks, [²²⁵Ac]Ac-GC33-BZM still demonstrates significant tumor uptake, suggesting that BZmacropa-NCS may be viable as a bifunctional chelator for in vivo studies of ²²⁵Ac-labeled antibody conjugates.

CONCLUSION

In summary, two rigid variants of the first-generation ²²⁵Ac chelator H₂macropa were synthesized by incorporating either one or two benzene rings into the macrocyclic base. Our comprehensive coordination chemistry studies of these ligands with La³⁺, a non-radioactive surrogate for Ac³⁺, revealed that they form complexes of lower stability than H₂macropa. DFT calculations were used to show that the use of phenyl groups in the backbone enhances their preorganization at the cost of their overall enthalpy of metal binding. These results highlight the different factors that need to be taken into consideration in designing and optimizing chelators for nuclear medicine applications. Despite their lower thermodynamic stability with La³⁺, ²²⁵Ac-radiolabeling studies with these ligands proceeded effectively, yielding high specific activity compounds within minutes at room temperature. Thus, these chelators are among the few candidates that can bind ²²⁵Ac under such mild conditions, rendering them valuable for use with sensitive macromolecular targeting vectors.

Based on these promising results, the bifunctional variant H₂BZmacropa-NCS was synthesized. In contrast to other large macrocyclic bifunctional chelators for ²²⁵Ac, H₂BZmacropa-NCS places the reactive functional group directly on the macrocycle rather than the pendent arms.

This design difference has two important implications. First, the synthetic approach is modular in that it allows for the installation of different pendent donor groups without perturbing the functional group handle on the macrocycle. Second, the stability of the –NCS functional group is substantially enhanced relative to that of the first-generation macropa-NCS. For this first-generation analogue, the –NCS group is installed on the pendent picolinate group and hydrolyzes rapidly both in the solid and solution state. These latter properties have made shipping and storage of this compound challenging. The enhanced hydrolytic stability of H₂BZmacropa-NCS, by contrast, should make it more accessible to other researchers. To further evaluate the suitability of this new bifunctional chelator, it was conjugated to the antibody GC33, which can be employed for targeting liver cancers that express GPC3. Consistent with our expectations based on the small-molecule chelators, radiolabeling of the GC33-BZM proceeded rapidly under mild, room temperature conditions. However, our serum stability and biodistribution studies revealed the ²²⁵Ac-labeled GC33-BZM to be less stable than the macropa conjugate, yet still capable of delivering this radionuclide to the tumor site. Although the serum and in vivo stability of the ²²⁵Ac-labeled GC33-BZM present some concerns, further optimization of this new bifunctional chelator, via modification of either the pendent donor arms or extension of the linker between the reactive –NCS group and the aromatic ring, may afford complexes of enhanced stability suitable for further clinical development. Alternatively, the use of H₂BZmacropa-NCS for other promising α -emitting radionuclides also warrants investigation. These efforts are currently underway within our labs.

ASSOCIATED CONTENT

Supporting Information

The Supporting Information is available free of charge on the ACS Publications website.

Synthetic procedures, experimental details, and supplementary figures. (PDF)

X-ray crystal data (CIF)

DFT optimized geometries (ZIP)

Notes

JJW and KJK are co-inventors on a provisional patent application on the use of the chelators reported in this manuscript for targeted alpha therapy applications.

ACKNOWLEDGMENT

A.P.K., S.F., K.E.B, and F.E.E acknowledge the support from Intramural Research Program funds ZIA BC 011800 and ZIA BC 010891. K.J.K. and J.J.W. were supported by Department of Energy Basic Energy Sciences (award No. DE-SC0021662) and National Institutes of Biomedical Imaging and Bioengineering of

the National Institutes of Health (award numbers R21EB027282 and R01EB02925). J.J.W also acknowledge the support from Research Corporation for Science Advancement through a Cottrell Research Scholar Award. We are grateful to Chugai Pharmaceutical for providing codrituzumab (GC33).

REFERENCES

- (1) Parker, C.; Nilsson, S.; Heinrich, D.; Helle, S. I.; O'Sullivan, J. M.; Fosså, S. D.; Chodacki, A.; Wiechno, P.; Logue, J.; Seke, M.; et al. Alpha Emitter Radium-223 and Survival in Metastatic Prostate Cancer. *N. Engl. J. Med.* **2013**, *369* (3), 213–223.
- (2) Abou, D. S.; Thiele, N. A.; Gutsche, N. T.; Villmer, A.; Zhang, H.; Woods, J. J.; Baidoo, K. E.; Escoria, F. E.; Wilson, J. J.; Thorek, D. L. J. Towards the Stable Chelation of Radium for Biomedical Applications with an 18-Membered Macroyclic Ligand. *Chem. Sci.* **2021**, *12* (10), 3733–3742.
- (3) Nelson, B. J. B.; Andersson, J. D.; Wuest, F. Targeted Alpha Therapy: Progress in Radionuclide Production, Radiochemistry, and Applications. *Pharmaceutics* **2021**, *13* (1), 49.
- (4) King, A. P.; Lin, F. I.; Escoria, F. E. Why Bother with Alpha Particles? *Eur. J. Nucl. Med. Mol. Imaging* **2021**, *49* (1), 7–17.
- (5) Thiele, N. A.; Wilson, J. J. Actinium-225 for Targeted α Therapy: Coordination Chemistry and Current Chelation Approaches. *Cancer Biother. Radiopharm.* **2018**, *33* (8), 336–348.
- (6) Yadav, M. P.; Ballal, S.; Sahoo, R. K.; Tripathi, M.; Seth, A.; Bal, C. Efficacy and Safety of ^{225}Ac -PSMA-617 Targeted Alpha Therapy in Metastatic Castration-Resistant Prostate Cancer Patients. *Theranostics* **2020**, *10* (20), 9364–9377.
- (7) Ballal, S.; Yadav, M. P.; Bal, C.; Sahoo, R. K.; Tripathi, M. Broadening Horizons with ^{225}Ac -DOTATATE Targeted Alpha Therapy for Gastroenteropancreatic Neuroendocrine Tumour Patients Stable or Refractory to ^{177}Lu -DOTATATE PRRT: First Clinical Experience on the Efficacy and Safety. *Eur. J. Nucl. Med. Mol. Imaging* **2020**, *47* (4), 934–946.
- (8) Tagawa, S. T.; Sun, M.; Sartor, A. O.; Thomas, C.; Singh, S.; Bissassar, M.; Fernandez, E.; Niaz, M. J.; Ho, B.; Vallabhajosula, S. et al. Phase I Study of ^{225}Ac -J591 for Men with Metastatic Castration-Resistant Prostate Cancer (MCRPC). *J. Clin. Oncol.* **2021**, *39* (15_suppl), 5015–5015.
- (9) Davis, I. A.; Glowienka, K. A.; Boll, R. A.; Deal, K. A.; Brechbiel, M. W.; Stabin, M.; Bochsler, P. N.; Mirzadeh, S.; Kennel, S. J. Comparison of ^{225}Ac Chelates: Tissue Distribution and Radiotoxicity. *Nucl. Med. Biol.* **1999**, *26* (5), 581–589.
- (10) Maguire, W. F.; McDevitt, M. R.; Smith-Jones, P. M.; Scheinberg, D. A. Efficient 1-Step Radiolabeling of Monoclonal Antibodies to High Specific Activity with ^{225}Ac for α -Particle Radioimmunotherapy of Cancer. *J. Nucl. Med.* **2014**, *55* (9), 1492–1498.
- (11) Mesude, B.; Katharina, L.; Teja, K.; Phelps, M. E.; Strand, S.; Morris, M. J.; Radu, C. G.; Damoiseaux, R.; Peltola, M. T.; Peekhaus, N.; et al. Genetic Signature of Prostate Cancer Mouse Models Resistant to Optimized HK2 Targeted α -Particle Therapy. *Proc. Natl. Acad. Sci.* **2020**, *117* (26), 15172–15181.
- (12) Lakes, A. L.; An, D. D.; Gauny, S. S.; Ansoborlo, C.; Liang, B. H.; Rees, J. A.; McKnight, K. D.; Karsunky, H.; Abergel, R. J. Evaluating ^{225}Ac and ^{177}Lu Radioimmunoconjugates against Antibody–Drug Conjugates for Small-Cell Lung Cancer. *Mol. Pharm.* **2020**, *17* (11), 4270–4279.
- (13) Sudo, H.; Tsuji, A. B.; Sugyo, A.; Kaneko, M. K.; Kato, Y.; Nagatsu, K.; Suzuki, H.; Higashi, T. Preclinical Evaluation of Podoplanin-Targeted Alpha-Radioimmunotherapy with the Novel Antibody NZ-16 for Malignant Mesothelioma. *Cells* **2021**, *10* (10), 2503.
- (14) Sudo, H.; Tsuji, A. B.; Sugyo, A.; Harada, Y.; Nagayama, S.; Katagiri, T.; Nakamura, Y.; Higashi, T. FZD10-Targeted α -Radioimmunotherapy with ^{225}Ac -Labeled OTSA101 Achieves Complete Remission in a Synovial Sarcoma Model. *Cancer Sci.* **2022**, *113* (2), 721–732.
- (15) Ramogida, C. F.; Robertson, A. K. H.; Jermilova, U.; Zhang, C.; Yang, H.; Kunz, P.; Lassen, J.; Bratanovic, I.; Brown, V.; Southcott, L.; et al. Evaluation of Polydentate Picolinic Acid Chelating Ligands and an α -Melanocyte-Stimulating Hormone Derivative for Targeted Alpha Therapy Using ISOL-Produced ^{225}Ac . *EJNMMI Radiopharm. Chem.* **2019**, *4* (1), 21.
- (16) Deal, K. A.; Davis, I. A.; Mirzadeh, S.; Kennel, S. J.; Brechbiel, M. W. Improved in Vivo Stability of Actinium-225 Macroyclic Complexes. *J. Med. Chem.* **1999**, *42* (15), 2988–2992.
- (17) Comba, P.; Jermilova, U.; Orvig, C.; Patrick, B. O.; Ramogida, C. F.; Rück, K.; Schneider, C.; Starke, M. Octadentate Picolinic Acid-Based Bispidine Ligand for Radiometal Ions. *Chem. Eur. J.* **2017**, *23* (63), 15945–15956.
- (18) Yang, H.; Zhang, C.; Yuan, Z.; Rodriguez-Rodriguez, C.; Robertson, A.; Radchenko, V.; Perron, R.; Gendron, D.; Causey, P.; Gao, F.; et al. Synthesis and Evaluation of a Macroyclic Actinium-225 Chelator, Quality Control and In Vivo Evaluation of ^{225}Ac -Crown-AMSH Peptide. *Chem. Eur. J.* **2020**, *26* (50), 11435–11440.
- (19) Hu, A.; Brown, V.; MacMillan, S. N.; Radchenko, V.; Yang, H.; Wharton, L.; Ramogida, C. F.; Wilson, J. J. Chelating the Alpha Therapy Radionuclides $^{225}\text{Ac}^{3+}$ and $^{213}\text{Bi}^{3+}$ with 18-Membered Macroyclic Ligands Macrodipa and Py-Macrodipa. *Inorg. Chem.* **2022**, *61* (2), 801–806.
- (20) Li, L.; Rousseau, J.; Jaraquemada-Peláez, M. de G.; Wang, X.; Robertson, A.; Radchenko, V.; Schaffer, P.; Lin, K.-S.; Bénard, F.; Orvig, C. ^{225}Ac -H4Py4pa for Targeted Alpha Therapy. *Bioconjug. Chem.* **2021**, *32* (7), 1348–1363.
- (21) Roca-Sabio, A.; Mato-Iglesias, M.; Esteban-Gómez, D.; Tóth, É.; Blas, A. de; Platas-Iglesias, C.; Rodríguez-Blas, T. Macroyclic Receptor Exhibiting Unprecedented Selectivity for Light Lanthanides. *J. Am. Chem. Soc.* **2009**, *131* (9), 3331–3341.
- (22) Clarke, E. T.; Martell, A. E. Stabilities of Trivalent Metal Ion Complexes of the Tetraacetate Derivatives of 12-, 13- and 14-Membered Tetraazamacrocycles. *Inorg. Chim. Acta* **1991**, *190* (1), 37–46.
- (23) Martell, , Smith, Robert M., A. E. *Critical Stability Constants. Volume 1*; Plenum Press: New York; London, 1974.
- (24) Thiele, N. A.; Brown, V.; Kelly, J. M.; Amor-Coarasa, A.; Jermilova, U.; MacMillan, S. N.; Nikolopoulou, A.; Ponnala, S.; Ramogida, C. F.; Robertson, A. K. H.; et al. An Eighteen-Membered Macroyclic Ligand for Actinium-225 Targeted Alpha Therapy. *Angew. Chem. Int. Ed.* **2017**, *56* (46), 14712–14717.
- (25) Hu, A.; Wilson, J. J. Advancing Chelation Strategies for Large Metal Ions for Nuclear Medicine Applications. *Acc. Chem. Res.* **2022**, *55* (6), 904–915.
- (26) Kelly, J. M.; Amor-Coarasa, A.; Ponnala, S.; Nikolopoulou, A.; Williams, C.; Thiele, N. A.; Schlyer, D.; Wilson, J. J.; DiMagno, S. G.; Babich, J. W. A Single Dose of ^{225}Ac -RPS-074 Induces a Complete Tumor Response in an LNCaP Xenograft Model. *J. Nucl. Med.* **2019**, *60* (5), 649–655.
- (27) Aluicio-Sarduy, E.; Thiele, N. A.; Martin, K. E.; Vaughn, B. A.; Devaraj, J.; Olson, A. P.; Barnhart, T. E.; Wilson, J. J.;

Boros, E.; Engle, J. W. Establishing Radiolanthanum Chemistry for Targeted Nuclear Medicine Applications. *Chem. Eur. J.* **2020**, *26* (6), 1238–1242.

(28) Reissig, F.; Bauer, D.; Zarschler, K.; Novy, Z.; Bendova, K.; Ludik, M.-C.; Kopka, K.; Pietzsch, H.-J.; Petrik, M.; Mamat, C. Towards Targeted Alpha Therapy with Actinium-225: Chelators for Mild Condition Radiolabeling and Targeting PSMA—A Proof of Concept Study. *Cancers.* **2021**, *13* (8), 1974.

(29) Bell, M. M.; Gutsche, N. T.; King, A. P.; Baidoo, K. E.; Kelada, O. J.; Choyke, P. L.; Escoria, F. E. Glypican-3-Targeted Alpha Particle Therapy for Hepatocellular Carcinoma. *Molecules* **2021**, *26* (1), 4.

(30) De Sousa, A. S.; Croft, G. J. B.; Wagner, C. A.; Michael, J. P.; Hancock, R. D. Effect of Cyclohexylene Bridges on the Metal Ion Size Based Selectivity of Ligands in Aqueous Solution. *Inorg. Chem.* **1991**, *30* (18), 3525–3529.

(31) Brechbiel, M. W.; Gansow, O. A. Synthesis of C-Functionalized Trans-Cyclohexyldiethylenetriaminepentacetic Acids for Labelling of Monoclonal Antibodies with the Bismuth-212 α -Particle Emitter. *J. Chem. Soc. Perkin Trans. 1* **1992**, *9*, 1173–1178.

(32) Ferreira-Martínez, R.; Esteban-Gómez, D.; Platas-Iglesias, C.; de Blas, A.; Rodríguez-Blas, T. Zn(II), Cd(II) and Pb(II) Complexation with Pyridinecarboxylate Containing Ligands. *Dalt. Trans.* **2008**, *42*, 5754–5765.

(33) Ramogida, C. F.; Cawthray, J. F.; Boros, E.; Ferreira, C. L.; Patrick, B. O.; Adam, M. J.; Orvig, C. H₂CHX₂Dedpa and H₄CHXOctapa—Chiral Acyclic Chelating Ligands for ^{67/68}Ga and ¹¹¹In Radiopharmaceuticals. *Inorg. Chem.* **2015**, *54* (4), 2017–2031.

(34) Wang, X.; Jaraquemada-Peláez, M. de G.; Cao, Y.; Ingham, A.; Rodríguez-Rodríguez, C.; Pan, J.; Wang, Y.; Saatchi, K.; Häfeli, U. O.; Lin, K.-S.; et al. H₂CHXHox: Rigid Cyclohexane-Reinforced Nonmacrocyclic Chelating Ligand for [Nat/^{67/68}Ga]Ga³⁺. *Inorg. Chem.* **2020**, *59* (7), 4895–4908.

(35) Hu, A.; Aluicio-Sarduy, E.; Brown, V.; MacMillan, S. N.; Becker, K. V.; Barnhart, T. E.; Radchenko, V.; Ramogida, C. F.; Engle, J. W.; Wilson, J. J. Py-Macrodipa: A Janus Chelator Capable of Binding Medicinally Relevant Rare-Earth Radiometals of Disparate Sizes. *J. Am. Chem. Soc.* **2021**, *143* (27), 10429–10440.

(36) Ishiguro, T.; Sugimoto, M.; Kinoshita, Y.; Miyazaki, Y.; Nakano, K.; Tsunoda, H.; Sugo, I.; Ohizumi, I.; Aburatani, H.; Hamakubo, T.; Kodama, T.; Tsuchiya, M.; Yamada-Okabe, H. Anti-Glypican 3 Antibody as a Potential Antitumor Agent for Human Liver Cancer. *Cancer Res.* **2008**, *68* (23), 9832–9838.

(37) Panchenko, P. A.; Zubenko, A. D.; Chernikova, E. Y.; Fedorov, Y. V.; Pashanova, A. V.; Karnoukhova, V. A.; Fedyanin, I. V.; Fedorova, O. A. Synthesis, Structure and Metal Ion Coordination of Novel Benzodiazamacrocyclic Ligands Bearing Pyridyl and Picolinate Pendant Side-Arms. *New J. Chem.* **2019**, *43* (38), 15072–15086.

(38) Thiele, N. A.; Woods, J. J.; Wilson, J. J. Implementing F-Block Metal Ions in Medicine: Tuning the Size Selectivity of Expanded Macrocycles. *Inorg. Chem.* **2019**, *58* (16), 10483–10500.

(39) Deblonde, G. J.-P.; Zavarin, M.; Kersting, A. B. The Coordination Properties and Ionic Radius of Actinium: A 120-Year-Old Enigma. *Coord. Chem. Rev.* **2021**, *446*, 214130.

(40) Corbaux, P.; Spiess, B.; Arnaud, F.; Schwing, M. J. Complexing Properties of an N,N'-Methylated Diaza-Crown-Ether. *Polyhedron* **1985**, *4* (8), 1471–1473.

(41) Fedorova, O.; Fedorov, Y.; Oshchepkov, M. Complexes of Di- and Triazacrown Ethers with Heavy Metal Ions in Water Solution. *Electroanalysis* **2012**, *24* (8), 1739–1744.

(42) Tei, L.; Baranyai, Z.; Botta, M.; Piscopo, L.; Aime, S.; Giovenzana, G. B. Synthesis and Solution Thermodynamic Study of Rigidified and Functionalised EGTA Derivatives. *Org. Biomol. Chem.* **2008**, *6* (13), 2361–2368.

(43) Wilson, J. J.; Ferrier, M.; Radchenko, V.; Maassen, J. R.; Engle, J. W.; Batista, E. R.; Martin, R. L.; Nortier, F. M.; Fassbender, M. E.; John, K. D.; et al. Evaluation of Nitrogen-Rich Macroyclic Ligands for the Chelation of Therapeutic Bismuth Radioisotopes. *Nucl. Med. Biol.* **2015**, *42* (5), 428–438.

(44) Hu, A.; MacMillan, S. N.; Wilson, J. J. Macroyclic Ligands with an Unprecedented Size-Selectivity Pattern for the Lanthanide Ions. *J. Am. Chem. Soc.* **2020**, *142* (31), 13500–13506.

(45) Vosjan, M. J. W. D.; Perk, L. R.; Visser, G. W. M.; Budde, M.; Jurek, P.; Kiefer, G. E.; van Dongen, G. A. M. S. Conjugation and Radiolabeling of Monoclonal Antibodies with Zirconium-89 for PET Imaging Using the Bifunctional Chelate p-Isothiocyanatobenzyl-Desferrioxamine. *Nat. Protoc.* **2010**, *5* (4), 739–743.

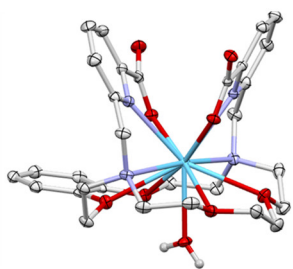
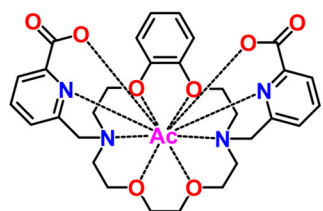
(46) Al-Ejeh, F.; Darby, J. M.; Thierry, B.; Brown, M. P. A Simplified Suite of Methods to Evaluate Chelator Conjugation of Antibodies: Effects on Hydrodynamic Radius and Biodistribution. *Nucl. Med. Biol.* **2009**, *36* (4), 395–402.

(47) Sharma, S. K.; Glaser, J. M.; Edwards, K. J.; Khozeimeh Sarbisheh, E.; Salih, A. K.; Lewis, J. S.; Price, E. W. A Systematic Evaluation of Antibody Modification and ⁸⁹Zr-Radiolabeling for Optimized Immuno-PET. *Bioconjug. Chem.* **2021**, *32* (7), 1177–1191.

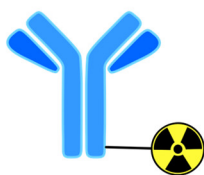
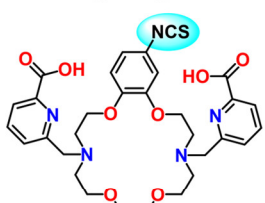
(48) Dadachova, E.; Chappell, L. L.; Brechbiel, M. W. Spectrophotometric Method for Determination of Bifunctional Macroyclic Ligands in Macroyclic Ligand–Protein Conjugates. *Nucl. Med. Biol.* **1999**, *26* (8), 977–982.

(49) Hooijman, E. L.; Chalashkan, Y.; Ling, S. W.; Kahyargil, F. F.; Segbers, M.; Bruchertseifer, F.; Morgenstern, A.; Seimbille, Y.; Koolen, S. L. W.; Brabander, T.; et al. Development of [²²⁵Ac]Ac-PSMA-I&T for Targeted Alpha Therapy According to GMP Guidelines for Treatment of MCRPC. *Pharmaceutics* **2021**, *13* (5), 715.

Ligand Design



Antibody Conjugation



Selective Tumor Accumulation

